

Features of the Pulsed Magnetization Switching in a High-Coercivity Material Based on ϵ -Fe₂O₃ Nanoparticles

S. I. Popkov^{a,*}, A. A. Krasikov^a, S. V. Semenov^a, A. A. Dubrovskii^a, S. S. Yakushkin^b,
V. L. Kirillov^b, O. N. Mart'yanov^b, and D. A. Balaev^a

^a Kirensky Institute of Physics, Krasnoyarsk Scientific Center, Siberian Branch, Russian Academy of Sciences, Krasnoyarsk, 660036 Russia

^b Boreskov Institute of Catalysis, Siberian Branch, Russian Academy of Sciences, Novosibirsk, 630090 Russia
*e-mail: psi@ksc.krasn.ru

Received October 17, 2019; revised October 17, 2019; accepted October 17, 2019

Abstract—The magnetic structure of the ϵ -Fe₂O₃ iron oxide polymorphic modification is collinear ferrimagnetic in the range from room temperature to ~ 150 K. As the temperature decreases, ϵ -Fe₂O₃ undergoes a magnetic transition accompanied by a significant decrease in the coercivity H_c and, in the low-temperature range, the compound has a complex incommensurate magnetic structure. We experimentally investigated the dynamic magnetization switching of the ϵ -Fe₂O₃ nanoparticles with an average size of 8 nm in the temperature range of 80–300 K, which covers different types of the magnetic structure of this iron oxide. A bulk material consisting of xerogel SiO₂ with the ϵ -Fe₂O₃ nanoparticles embedded in its pores was examined. The magnetic hysteresis loops under dynamic magnetization switching were measured using pulsed magnetic fields H_{\max} of up to 130 kOe by discharging a capacitor bank through a solenoid. The coercivity H_c upon the dynamic magnetization switching noticeably exceeds the H_c value under the quasi-static conditions. This is caused by the superparamagnetic relaxation of magnetic moments of particles upon the pulsed magnetization switching. In the range from room temperature to ~ 150 K, the external field variation rate dH/dt is the main parameter that determines the behavior of the coercivity under the dynamic magnetization switching. It is the behavior that is expected for a system of single-domain ferro- and ferrimagnetic particles. Under external conditions (at a temperature of 80 K) when the ϵ -Fe₂O₃ magnetic structure is incommensurate, the coercivity during the pulsed magnetization switching depends already on the parameter dH/dt and is determined, to a great extent, by the maximum applied field H_{\max} . Such a behavior atypical of systems of ferrimagnetic particles is caused already by the dynamic spin processes inside the ϵ -Fe₂O₃ particles during fast magnetization switching.

Keywords: ϵ -Fe₂O₃ nanoparticles, dynamic magnetization switching, coercivity

DOI: 10.1134/S1063783420030166

1. INTRODUCTION

Ferric iron oxide ϵ -Fe₂O₃ is a material with the unique magnetic properties. This iron oxide polymorph only exists in the form of nanoparticles up to ~ 20 – 30 nm in size and exhibits a coercivity of about 20 kOe at room temperature [1–8], which is a record for magnetic nanoparticles of such sizes [5]. This circumstance, together with the property related to the high coercivity—the effective absorption of electromagnetic waves in the millimeter range [9, 10]—make the materials based on the ϵ -Fe₂O₃ nanoparticles promising for applications.

Iron atoms in the ϵ -Fe₂O₃ structure occupy four nonequivalent sites. According to the recent investigations [11, 12], the magnetic order in ϵ -Fe₂O₃ is maintained at temperatures of up to ~ 850 K (two of the four

sublattices of Fe atoms are ordered [11]). In the vicinity of ~ 500 K, all four sublattices are already ordered into a collinear ferrimagnetic structure [11], which exists at temperatures of up to ~ 150 K (the hard-magnetic phase). However, in the range of 80–150 K, structural distortions induce a stepwise magnetic transition [13, 14] into some incommensurate magnetic structure [14]. In this case, a sharp decrease in the coercivity occurs in the above-mentioned temperature range. Therefore, despite a twenty-year history of intense research (ϵ -Fe₂O₃ was reliably obtained first in 1998 [15]), some questions of understanding the magnetic structure of this oxide still remain open. One of the problems is the ϵ -Fe₂O₃ magnetic state at low (up to 80 K) temperatures.

The pulsed magnetization switching (the main method used in this study) is a particular case of study-

ing the dynamic magnetic hysteresis (DMH). The latter involves the study of the effect of frequency ν of an ac magnetic field

$$H = H_{\max} \sin(2\pi\nu t) \quad (1)$$

on the parameters of the hysteresis loop (H_c , loop area, etc.). In bulk materials, the dynamic hysteresis is mainly determined by processes that occur in the domain structure, while in single-domain ferro- and ferrimagnetic particles, the dynamic hysteresis is related to the relaxation of the particle magnetic moment and depends on the particle size, magnetic structure, and magnetic anisotropy [16–18]. The DMH behavior is related to the application in hyperthermia [19, 20] and magnetic memory [21, 22]. Therefore, the DMH investigations are important and promising for studying the magnetic state of nanoparticle systems.

We would like to note one fact important for studying the DMH. Conventional facilities generating an ac magnetic field impose significant limitations on the maximum applied field H_{\max} and frequency ν . These limitations are related to the power released in a solenoid. Therefore, at frequencies of 10^2 – 10^3 Hz, it is difficult to obtain the H_{\max} values higher than $\sim 10^3$ Oe. This circumstance complicates the DMH investigations in materials with the high magnetic anisotropy, since, if H_{\max} is significantly lower than the field H_{irr} of the irreversible magnetization behavior, then the resulting hysteresis loop will be minor. Consequently, the obtained parameters (H_c and remanent magnetization) will be determined mainly by the minor hysteresis loop. An alternative to the conventional methods for studying the DMH is the use of pulsed fields in which the power release is limited to a single cycle of the external field variation, so it becomes possible to increase the maximum applied field to hundreds of kilooersteds.

In $\epsilon\text{-Fe}_2\text{O}_3$, the H_{irr} value attains ~ 60 kOe [3, 5, 23]; therefore, the dynamic magnetization switching in the $\epsilon\text{-Fe}_2\text{O}_3$ nanoparticles can only be studied using pulsed fields. Previously, we examined the dynamic magnetization switching of the $\epsilon\text{-Fe}_2\text{O}_3$ nanoparticles with an average size of ~ 10 nm at temperatures of 300 and 77 K [24]. The dependences of the coercivity on the external field variation rate dH/dt were analyzed using the theoretical model for the dynamic magnetization switching of ferromagnetic nanoparticles [25, 26]. This made it possible to unambiguously extract the contribution of the surface magnetic anisotropy to the formation of the dynamic properties of nanoparticles of this oxide [24]. The model [25, 26] described well the room-temperature experimental results, while at 77 K a significant discrepancy between the theoretical and experimental dependences of H_c on dH/dt was observed [24]. To establish the temperature evolution

of the dynamic coercivity and elucidate the origin of the discrepancy between the model and the experiment at $T = 77$ K, here we investigate the pulsed magnetization switching of a material based on the $\epsilon\text{-Fe}_2\text{O}_3$ nanoparticles with an average size of ~ 8 nm. The measurement range is 80–300 K, which covers both the hard-magnetic phase (the temperature range of its existence is 150–500 K) and the complex (not exactly established yet) incommensurate magnetic structure at 80 K, which forms after the magnetic transition in the temperature range of 80–150 K.

2. EXPERIMENTAL

2.1. Synthesis and Characterization of the $\epsilon\text{-Fe}_2\text{O}_3$ Nanoparticle/SiO₂ Xerogel Sample

We studied a sample containing 20 wt % of $\epsilon\text{-Fe}_2\text{O}_3$ in the SiO₂ xerogel matrix. The sample was synthesized by a method that was implemented first and described in detail in [27]. The powder diffraction pattern was obtained on a D8 Advance Bruker diffractometer (Germany) in $\text{CuK}\alpha$ radiation at a wavelength of 1.5418 Å. Micrographs of the particles were obtained on a JEOL JEM-2010 electron microscope at an accelerating voltage of 200 kV with a resolution of 1.4 Å.

According to the X-ray diffraction data, all the observed diffraction peaks belong to the $\epsilon\text{-Fe}_2\text{O}_3$ structure (Fig. 1a). The high-resolution transmission electron microscopy data (Fig. 1c) showed that the average particle size was 8 nm. A histogram of the particle size distribution obtained using a great number of shots is shown in Fig. 1b. In addition, the analysis of the Mössbauer spectra showed that the sample does not contain any polymorphic modifications of iron oxide, except for $\epsilon\text{-Fe}_2\text{O}_3$ [27, 28].

We note that the samples consisting of the $\epsilon\text{-Fe}_2\text{O}_3$ nanoparticles in the SiO₂ xerogel matrix are bulk centimeter-sized wafers. This allowed us to perform the measurements in magnetic fields without special fixing the nanoparticles, which is necessary for powder samples.

2.2. Measuring the Quasi-Static Magnetic Properties

The quasi-static magnetic properties were measured on a vibrating sample (VSM) magnetometer [29]. The temperature dependences of the magnetization $M(T)$ were measured under the zero external field cooling (ZFC) and field cooling (FC) conditions. The field dependences of the magnetization $M(H)$ were measured under the ZFC conditions. The field variation rate $(dH/dt)_{\text{VSM}}$ during the measurements of the quasi-static hysteresis loops $M(H)$ was ≈ 50 Oe/s. To obtain the dependence of H_c on the maximum applied field H_{\max} , we measured a family of minor hysteresis

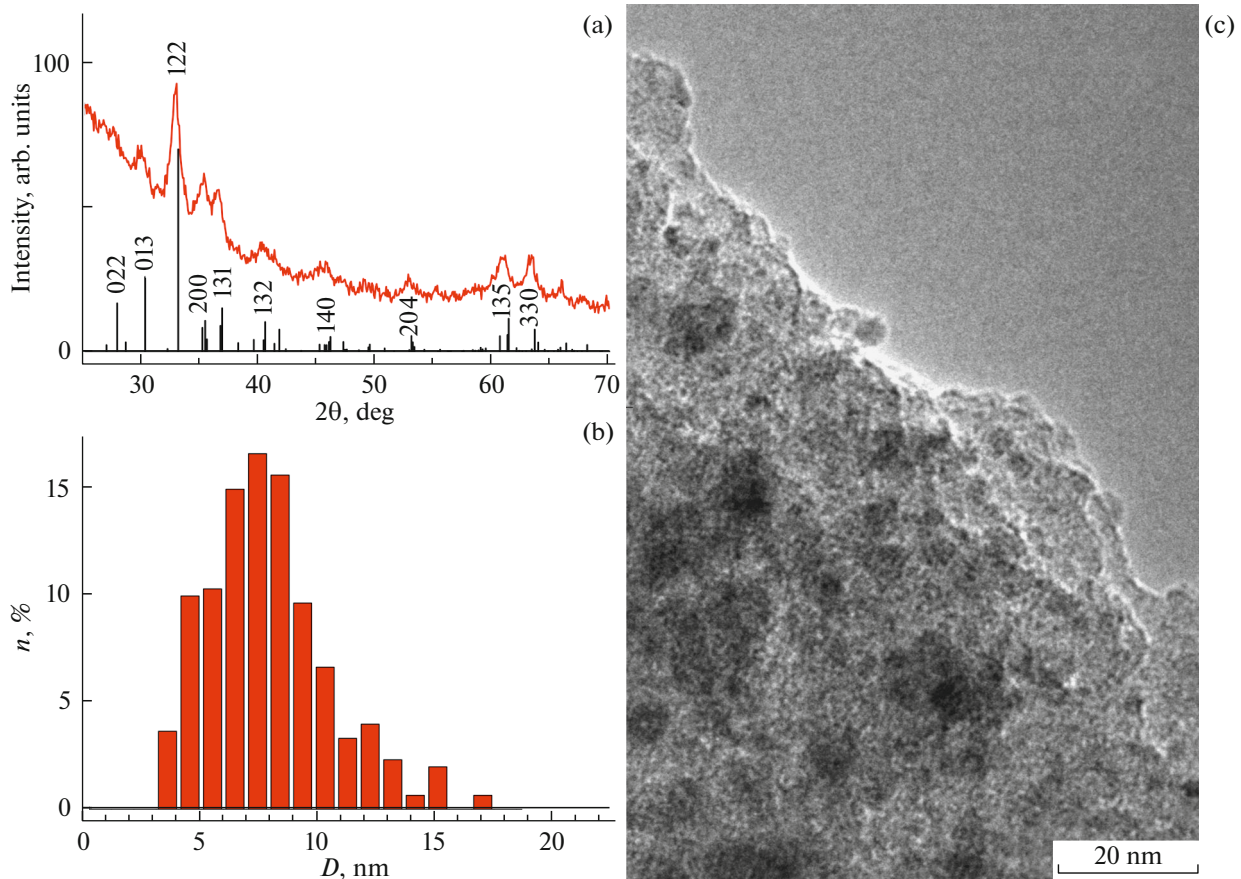


Fig. 1. (a) X-ray diffraction pattern of the investigated sample, (b) particle size distribution, and (c) typical transmission electron microscopy micrograph of a particle.

loops with a gradually increasing H_{\max} value. The magnetization values were normalized to the iron oxide mass in the sample.

2.3. Measuring the Dynamic Magnetic Hysteresis Loops upon Pulsed Magnetization Switching

In the DMH study, we used an original strong pulsed field facility (Kirensky Institute of Physics, Siberian Branch, Russian Academy of Sciences) using a technique of capacitor bank discharging through a solenoid. Usually, the oscillatory process in such facilities is stopped by a thyristor after the first half-wave, while the measurements of the magnetization hysteresis loops require at least two half-waves. To form the second half-wave, diodes were connected in the facility circuit antiparallel to the thyristor circuit. Figure 2 shows typical time dependences of the field in the solenoid for different maximum fields (determined by the capacitor charging voltage), pulse length, and half-wave time τ_p . The latter was changed by switching the capacitor banks to different capacities. The measurements were performed at τ_p values of 4, 8, and 16 ms.

The zero field value at the time $t = \tau_p$ is due to the thyristor block closing.

To measure the magnetization, we used an inductive sensor representing a system of coaxial compensated coils into which the sample was placed. The signal induced in the coils was amplified and recorded by a digital storage oscillograph. The measurements were performed in the temperature range of 80–300 K. At constant temperature, in each next measurement, the H_{\max} value was greater than the previous one. The magnetization data obtained in pulsed fields were compared with the hysteresis loops measured by the VSM technique.

3. RESULTS AND DISCUSSION

Figure 3 shows ZFC and FC temperature dependences of the magnetization $M(T)$ for the investigated sample. The observed nonmonotonic behavior of the $M(T)$ dependences (the maxima at 110–120 K) is not a manifestation of the superparamagnetic blocking. The superparamagnetic blocking temperature for the ϵ - Fe_2O_3 particles with a size of 6 nm and more is much higher than room temperature [23, 28, 30, 31]. The

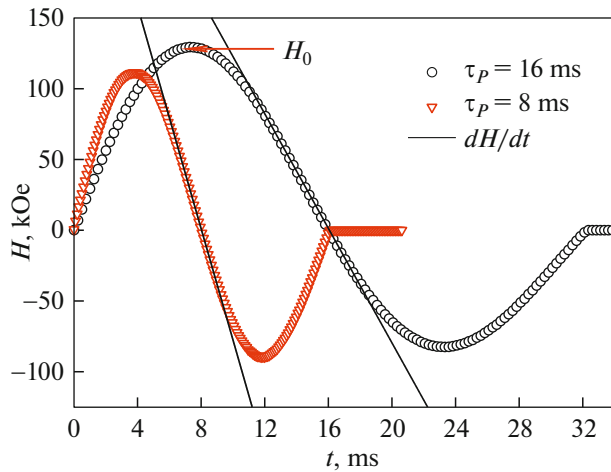


Fig. 2. Typical time dependence of the solenoid field in the pulsed technique at different maximum applied fields H_0 and indicated pulse lengths τ_p . The slopes of the straight lines correspond to the field variation rates dH/dt at the moment of magnetization switching in the sample.

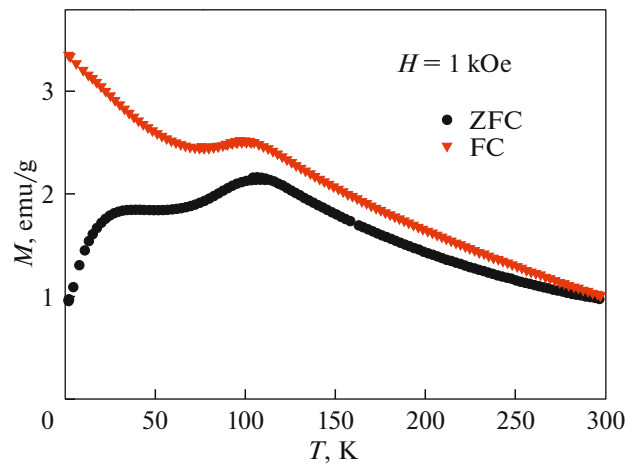


Fig. 3. Temperature dependences of magnetization for the investigated sample of the ϵ - Fe_2O_3 nanoparticles at different thermomagnetic prehistories in a field of $H = 1$ kOe (ZFC is the zero external field cooling mode and FC is the field cooling mode).

pronounced anomalies in the vicinity of 120 K in Fig. 3 and the change in the $M(T)$ behavior near 80 K are indicative of the magnetic transition that is known to occur in ϵ - Fe_2O_3 in the temperature range of 80–150 K [3, 13, 14].

This magnetic transition is reflected also in the temperature behavior of the coercivity. Figure 4 shows the $H_C(T)$ dependence obtained from the measured magnetic hysteresis loops under the quasi-static conditions (VSM). A fairly sharp decrease in the coercivity caused by the magnetic transition begins at ~ 150 K (with a decrease in temperature). It is noteworthy that the relatively low H_C values (~ 3 kOe at room temperature) for the investigated sample are caused by a sufficiently small (8 nm) particle size [5, 23, 32, 33]. The ϵ - Fe_2O_3 particles ~ 10 and 20 nm in size exhibit a coercivity of about 10 and 20 kOe, respectively [5, 33].

During the pulsed field measurements (Fig. 2), parts of the hysteresis loop are detected in the field ranges (i) from $H = 0$ to H_{\max} , (ii) from H_{\max} to the negative field $-H_m$ slightly weaker than $|H_{\max}|$ (damped oscillations in the LCR circuit), and, then, (iii) from $-H_m$ to zero field. In this technique, the most informative part of the $M(H)$ dependence is portion (ii); therefore, in the analysis of the pulsed magnetization switching data, we will use this $M(H)$ portion (the negative field region). Figures 5a and 6a show typical hysteretic $M(H)$ dependences for the investigated samples obtained at $T = 80$ and 300 K, respectively. The figures present the VSM quasi-static magnetometry data (at $H_{\max} = 60$ kOe) and the $M(H)$ dependences obtained by pulsed magnetometry at the τ_p and H_{\max} values indicated in the figures. Figures 5b and 6b illustrate a typical behavior of the hysteresis

loops ($T = 80$ K in Fig. 5b and $T = 300$ K in Fig. 6b) near the origin of coordinates for the techniques used. The hysteresis loops obtained by pulsed magnetization switching are noticeably wider than those in the VSM technique. All the data obtained by the pulsed magnetization switching reveal the broadening of the hysteresis loops both with an increase in H_{\max} and with a decrease in the pulse length τ_p . Next, we will operate with the coercivity H_C in the negative field region determined as a point of intersection of the $M(H)$ dependence with the abscissa axis in the negative field region.

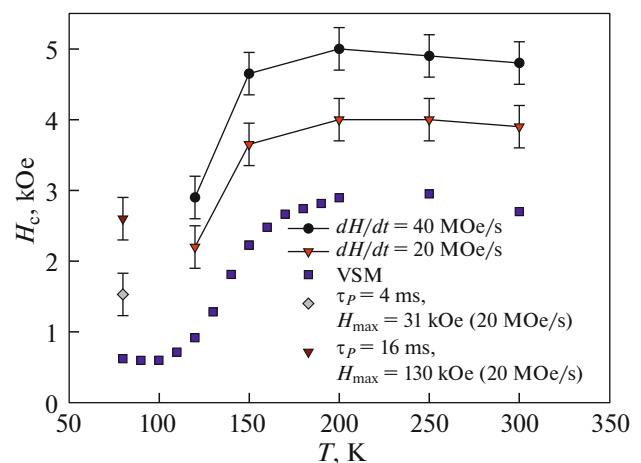


Fig. 4. Temperature evolution of the coercivity H_C for the quasi-static (VSM) measurements of the magnetization hysteresis and under pulsed magnetization switching for the indicated parameters.

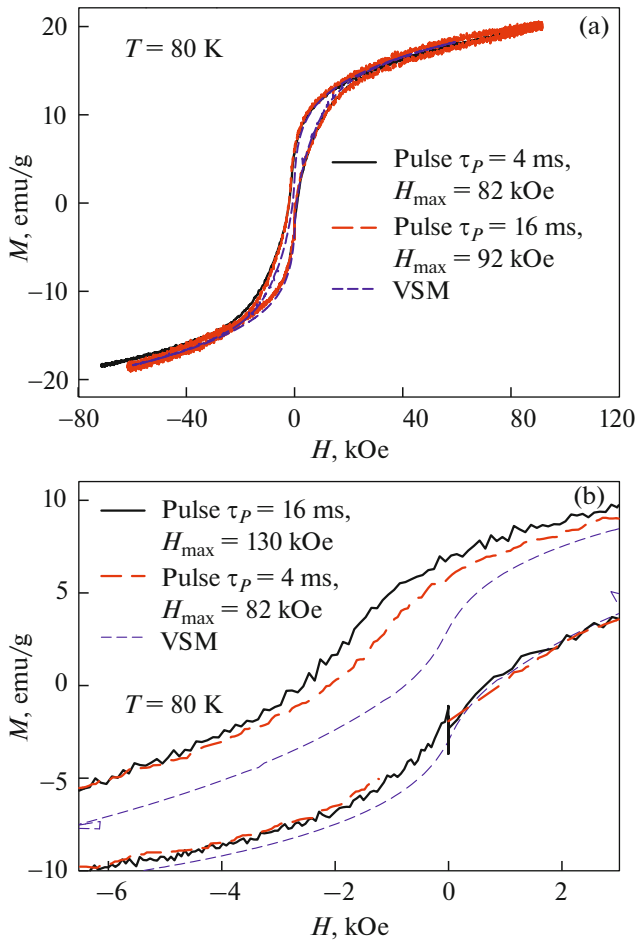


Fig. 5. (a) Typical hysteresis loops of the investigated sample of the ϵ - Fe_2O_3 nanoparticles obtained by the VSM technique and in pulsed fields at different momentum parameters and a temperature of 300 K. (b) Behavior of the $M(H)$ dependences in the vicinity of the origin of coordinates. The τ_p and H_{\max} values are shown in the figures.

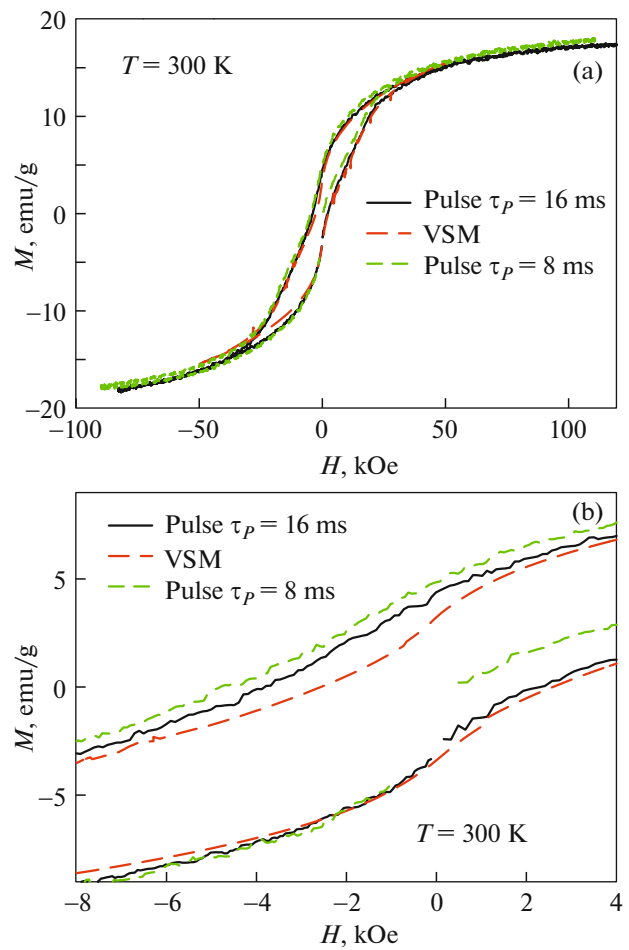


Fig. 6. (a) Typical hysteresis loops of the investigated sample of ϵ - Fe_2O_3 nanoparticles, obtained by the VSM technique and in pulsed fields at different pulse parameters and a temperature of 80 K. (b) Behavior of the $M(H)$ dependences in the vicinity of the origin of coordinates. The τ_p and H_{\max} values are shown in the figures.

In the theoretical consideration of the DMH, the area of the hysteresis loop is determined (*ceteris paribus*) by the ac field frequency [16, 17, 25, 26] and the H_{\max} value. Both these parameters determine the rate of variation in the external field $dH(t)/dt$, which, at harmonic law (1) being valid, yields the equality $dH(t)/dt = 2\pi\nu H_{\max} \cos(2\pi\nu t)$. If we consider only one parameter of the hysteresis loop (the coercivity), then, at $H_c \ll H_{\max}$, the dH/dt value corresponds with good accuracy to the slope of the tangent to the $H(t)$ dependence (Fig. 2). In our experiments, the H_{\max} and τ_p values vary; in the notation used for pulse techniques, $\nu = 1/2\tau_p$ (see also Fig. 2). Therefore, in the vicinity of $H = 0$, the external field variation rate will be

$$dH/dt = H_{\max}/2\tau_p. \quad (2)$$

We focus on the dependence of the coercivity on dH/dt and on the variable parameters of the momen-

tum (τ_p and H_{\max}). Figure 7 presents the dependences of H_c on dH/dt (Figs. 7a, 7c) and on H_{\max} (Figs. 7b, 7d) for the $M(H)$ dependences obtained at temperatures of 80 and 300 K. For a temperature of 300 K in the coordinates H_c and dH/dt , the data for the two pulse lengths fall on one functional dependence (Fig. 7a). This gives us grounds to consider the ϵ - Fe_2O_3 nanoparticles to be single-domain ferrimagnetic particles [3, 24] and apply the theoretical model [25, 26] developed for ferromagnetic particles to the results obtained. In addition, due to the validity of Eq. (2), the experimental data in the coordinates H_c and H_{\max} are divided into two dependences corresponding to different pulse lengths: at $H_{\max} \approx \text{const}$ $H_c(\tau_p = 8 \text{ ms}) > H_c(\tau_p = 16 \text{ ms})$ in Fig. 7b. The described behavior (unambiguity of the $H_c(dH/dt)$ dependence) is observed at temperatures from room to 120–150 K. Therefore, the magnetization switching rate dH/dt is

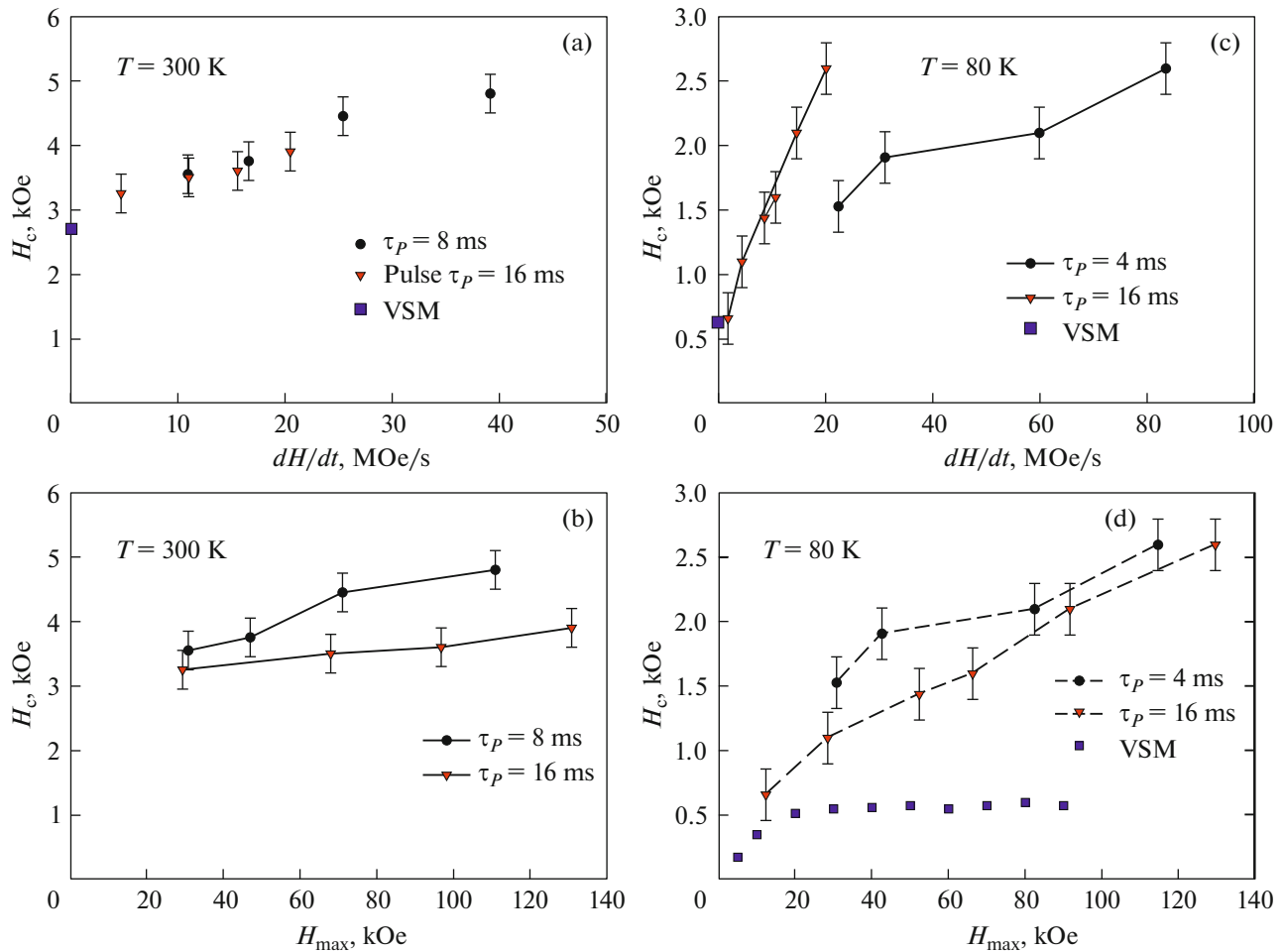


Fig. 7. Coercivity H_c under the pulsed magnetization switching as a function of (a, c) the dH/dt and (b, d) H_{max} parameters for the sample of ϵ -Fe₂O₃ nanoparticles at temperatures of (a, b) 300 and (c, d) 80 K at the indicated pulse lengths τ_p . (b, c, d) Data for the same pulse length are grouped by the connecting lines. (a, c, d) VSM data.

the parameter that unambiguously determines the coercivity of single-domain ferro- and ferrimagnetic nanoparticles during the dynamic magnetization switching.

The data obtained in the region below the magnetic transition (at 80 K) reveal a fundamentally different behavior of the coercivity upon variation in the pulse parameters. The dependence of H_c on dH/dt is no longer an unambiguous function for the data at different pulse lengths (see Fig. 7c). On the contrary, the data in Fig. 7c are divided into two dependences for each τ_p value, which are rather far from one another. At the same time, in the coordinates H_c and H_{max} , the groups of points for different τ_p values are close to each other (Fig. 7d), although the inequality $H_c(\tau_p = 4 \text{ ms}) > H_c(\tau_p = 16 \text{ ms})$ is valid. We may conclude that, for the data obtained at a temperature of 80 K, there is no universal parameter determining the coercivity.

A behavior similar to the data obtained at a temperature of 80 K (Figs. 7c, 7d) was observed by us in NiO antiferromagnetic nanoparticles [34] and ferrihydrite nanoparticles [35]. In nanosized antiferromagnetic particles, the magnetization hysteresis is caused by their uncompensated magnetic moment induced by structural defects and surface effects [36–40]. The presence of not one (antiferromagnetic), but two or more magnetic subsystems in antiferromagnetically ordered nanoparticles, as well as the interaction between them, can cause the observed strong fields of the irreversible behavior (H_{irr}) of the magnetization curves of such objects [41–43]. This leads to the fact that the $H_c(H_{max})$ dependence for antiferromagnetic nanoparticles does not saturate and the magnetic hysteresis loops remain open at $H_{max} < H_{irr}$. As a consequence, in pulsed fields the maximum applied field H_{max} is more important than in Eq. (2).

The above-mentioned analogy with antiferromagnetic nanoparticles would be a reasonable explanation

of the behavior observed in ϵ -Fe₂O₃ if we recognize that it is the defects in this iron oxide that lead to the presence of a magnetic moment in the particles. However, the magnetization hysteresis for the ϵ -Fe₂O₃ particles larger than 6 nm is observed over the entire temperature range (including the discussed temperature of 80 K). Moreover, under the quasi-stationary conditions at 80 K, the $H_c(H_{\max})$ dependence saturates in fields of about 30–40 kOe (see the VSM data in Fig. 7d), which does not allow as to draw an unambiguous analogy between antiferromagnetic nanoparticles and the ϵ -Fe₂O₃ nanoparticles. At temperatures of 80 and 300 K, for which the obtained $H_c(dH/dt)$ and $H_c(H_{\max})$ dependences are discussed, the ϵ -Fe₂O₃ magnetic structure is different. At room temperature, ϵ -Fe₂O₃ is a collinear ferrimagnet and the magnetization hysteresis behavior can be described within the classical consideration of the Stoner–Wohlfahrt model [44], while after the magnetic transition in the range of 80–150 K, the ϵ -Fe₂O₃ magnetic structure becomes incommensurate [3, 14]. Therefore, we may conclude that the magnetic structure change dramatically affects the coercivity behavior under the pulsed magnetization switching.

The aforesaid elucidates the origin of the discrepancy between the experimental $H_c(dH/dt)$ dependence obtained in [24] for the ϵ -Fe₂O₃ particles ~10 nm in size at a temperature of 77 K and the theoretical model from [25, 26], which considers single-domain ferro- or ferrimagnetic particles. In a systems of single-domain ferro- or ferrimagnetic particles, the resulting (hysteretic) magnetization curve corresponds to the arrangement of the magnetic moments of the entire particle along the field (the competition of the Zeeman and magnetic anisotropy energies). In this case, the magnetic moment of an individual particle is considered to be invariable (determined by magnetic ordering inside a particle). For a complex incommensurate magnetic structure, an additional contribution is quite possible, specifically, a partial rotation of the spins of iron atoms already inside a particle. This process can be dynamic; i.e., the angle of rotation of the spins (taking into account averaging at the random orientation of the crystallographic axes) in the incommensurate magnetic structure will substantially depend on the magnetization switching time. Then, it is reasonable that the dH/dt parameter will not be the main parameter determining the magnetization and magnetization switching processes, while the pulse length is more important than at the ferrimagnetic order inside a particle. We note that, in [13, 45], the anomalous dependences of the ac susceptibility χ on the frequency of the applied field were observed in the temperature range of 80–100 K: the $\chi(T)$ maximum shifted toward lower temperatures with increasing ac field frequency. This indirectly confirms our arguments that it is the change in the magnetic structure that leads to the observed atypical behavior of the

coercivity of single-domain ferrimagnetic particles under the dynamic magnetization switching.

The temperature evolution of the coercivity of the investigated sample under the pulsed magnetization switching is shown in Fig. 4. Together with the $H_c(T)$ dependence obtained by the VSM technique, the figure presents the dH/dt data (20 and 40 MOe/s). It can be seen that, in the range from room temperature to ~120–150 K, the behavior of the dynamic coercivity is similar to that observed under the quasi-static conditions. A sufficiently sharp decrease in the coercivity starts at ~150 K (with a decrease in temperature), which is caused by the magnetic transition. Since at a temperature of 80 K the dH/dt parameter is no longer universal for describing the dynamic coercivity, Fig. 4 shows the H_c values for this temperature obtained at $H_{\max} = 31$ and 130 kOe and $\tau_p = 4$ and 16 ms, respectively (these parameters correspond to a dH/dt value of 20 MOe/s).

4. CONCLUSIONS

Thus, the magnetization switching of the ϵ -Fe₂O₃ nanoparticles with an average size of 8 nm in pulsed fields in the temperature range of 80–300 K was experimentally studied. In the range from room temperature to 150 K, in which ϵ -Fe₂O₃ has a collinear ferrimagnetic structure, the behavior typical of single-domain ferro- and ferrimagnetic particles is observed; i.e., the coercivity increases with the field variation rate dH/dt and this parameter is most important for describing the dynamic magnetization switching. The temperature evolution of the dynamic coercivity is similar to that under the quasi-static magnetization switching. At a temperature of 80 K, i.e., below the well-known magnetic transition in ϵ -Fe₂O₃ (in the range of 80–150 K), the behavior of the coercivity can no longer be described by only the dH/dt parameter. An important, if not decisive, role is played here by the maximum applied field H_{\max} . We can state that the drastic change in the magnetic structure caused by the magnetic transition no longer allows one to consider the ϵ -Fe₂O₃ particles to be single-domain ferrimagnetic. The observed behavior is a distinguishing feature of the change in the ϵ -Fe₂O₃ magnetic structure after the magnetic transition, which is important for understanding of the magnetic phase diagram of ϵ -Fe₂O₃.

FUNDING

The study was supported by the Russian Foundation for Basic Research, the Government of the Krasnoyarsk Krai, and the Krasnoyarsk Territorial Foundation for Support of Scientific and R&D Activities, project no. 18-42-240012 “Magnetization Switching of Magnetic Nanoparticles in Strong Pulsed Magnetic Fields: New Approach to Studying

the Dynamic Effects Related to the Magnetization of Magnetic Nanoparticles.”

CONFLICT OF INTEREST

The authors declare that they have no conflicts of interest.

REFERENCES

- J. Tuček, R. Zboril, A. Namai, and S. Ohkoshi, *Chem. Mater.* **22**, 6483 (2010).
- L. Machala, J. Tuček, and R. Zboril, *Chem. Mater.* **23**, 3255 (2011).
- M. Gich, A. Roig, C. Frontera, E. Molins, J. Sort, M. Popovici, G. Chouteau, D. Martín y Marero, and J. Nogués, *J. Appl. Phys.* **98**, 044307 (2005).
- S. Sakurai, S. Kuroki, H. Tokoro, K. Hashimoto, and S. Ohkoshi, *Adv. Funct. Mater.* **17**, 2278 (2007).
- S. Ohkoshi, A. Namai, K. Imoto, M. Yoshikiyo, W. Tarora, K. Nakagawa, M. Komine, Y. Miyamoto, T. Nasu, S. Oka, and H. Tokoro, *Sci. Rep.* **5**, 14414 (2015).
- S. Ohkoshi, S. Kuroki, S. Sakurai, K. Matsumoto, K. Sato, and S. Sasaki, *Angew. Chem. Int. Ed.* **46**, 8392 (2007).
- A. I. Dmitriev, O. V. Koplak, A. Namai, H. Tokoro, S. Ohkoshi, and R. B. Morgunov, *Phys. Solid State* **56**, 1795 (2014).
- S. Ohkoshi, A. Namai, T. Yamaoka, M. Yoshikiyo, K. Imoto, T. Nasu, S. Anan, Y. Umetsu, K. Nakagawa, and H. Tokoro, *Sci. Rep.* **6**, 27212 (2016).
- A. Namai, S. Sakurai, M. Nakajima, T. Suemoto, K. Matsumoto, M. Goto, S. Sasaki, and S. Ohkoshi, *J. Am. Chem. Soc.* **131**, 1170 (2009).
- S. Ohkoshi, S. Kuroki, S. Sakurai, K. Matsumoto, K. Sato, and S. Sasaki, *Angew. Chem. Int. Ed.* **46**, 8392 (2007).
- J. L. García-Muñoz, A. Romaguera, F. Fauth, J. Nogués, and M. Gich, *Chem. Mater.* **29**, 9705 (2017).
- D. A. Balaev, A. A. Dubrovskiy, S. S. Yakushkin, G. A. Bukhtiyarova, and O. N. Mart'yanov, *Phys. Solid State* **61**, 345 (2019).
- M. Kurmoo, J.-L. Rehspringer, A. Hutlova, C. D'Orlans, S. Vilminot, C. Estournes, and D. Niznansky, *Chem. Mater.* **17**, 1106 (2005).
- M. Gich, C. Frontera, A. Roig, E. Taboada, E. Molins, H. R. Rechenberg, J. D. Ardisson, W. A. A. Macedo, C. Ritter, V. Hardy, J. Sort, V. Skumryev, and J. Nogués, *Chem. Mater.* **18**, 3889 (2006).
- E. Tronc, S. Chaneac, and J. P. Jolivet, *J. Solid State Chem.* **139**, 93 (1998).
- N. A. Usov and Yu. B. Grebenshchikov, *J. Appl. Phys.* **106**, 023917 (2009).
- E. L. Verde, G. T. Landi, J. A. Gomes, M. H. Sousa, and A. F. Bakuzis, *J. Appl. Phys.* **111**, 123902 (2012).
- J. Carrey, B. Mehdaoui, and M. Respaud, *J. Appl. Phys.* **109**, 083921 (2011).
- A. S. Kamzin, D. S. Nikam, and S. H. Pawar, *Phys. Solid State* **59**, 156 (2017).
- A. S. Kamzin, *Phys. Solid State* **58**, 532 (2016).
- A. M. Shut'yi and D. I. Sementsov, *Phys. Solid State* **61**, 1736 (2019).
- A. M. Shut'yi and D. I. Sementsov, *J. Exp. Theor. Phys.* **129**, 248 (2019).
- A. A. Dubrovskiy, D. A. Balaev, K. A. Shaykhutdinov, O. A. Bayukov, O. N. Pletnev, S. S. Yakushkin, G. A. Bukhtiyarova, and O. N. Mart'yanov, *J. Appl. Phys.* **118** (2015).
- D. A. Balaev, I. S. Poperechny, A. A. Krasikov, K. A. Shaikhutdinov, A. A. Dubrovskiy, S. I. Popkov, A. D. Balaev, S. S. Yakushkin, G. A. Bukhtiyarova, O. N. Mart'yanov, and Yu. L. Raikher, *J. Appl. Phys.* **117**, 063908 (2015).
- I. S. Poperechny, Yu. L. Raikher, and V. I. Stepanov, *Phys. Rev. B* **82**, 174423 (2010).
- I. S. Poperechny, Yu. L. Raikher, and V. I. Stepanov, *Phys. B (Amsterdam, Neth.)* **435**, 58 (2014).
- S. S. Yakushkin, D. A. Balaev, A. A. Dubrovskiy, S. V. Semenov, Yu. V. Knyazev, O. A. Bayukov, V. L. Kirillov, R. D. Ivantsov, I. S. Edelman, and O. N. Mart'yanov, *Ceram. Int.* **44**, 17852 (2018).
- Yu. V. Knyazev, D. A. Balaev, V. L. Kirillov, O. A. Bayukov, and O. N. Mart'yanov, *JETP Lett.* **108**, 527 (2018).
- A. D. Balaev, Yu. V. Boyarshinov, M. M. Karpenko, and B. P. Khrustalev, *Prib. Tekh. Eksp.*, No. 3, 167 (1985).
- S. S. Yakushkin, A. A. Dubrovskiy, D. A. Balaev, K. A. Shaykhutdinov, G. A. Bukhtiyarova, and O. N. Mart'yanov, *J. Appl. Phys.* **111**, 44312 (2012).
- I. Edelman, J. Kliava, O. Ivanova, R. Ivantsov, D. Velikanov, V. Zaikovskii, E. Petrakovskaja, Y. Zubavichus, and S. Stepanov, *J. Non-Cryst. Solids* **506**, 68 (2019).
- O. S. Ivanova, R. D. Ivantsov, I. S. Edelman, E. A. Petrakovskaja, D. A. Velikanov, Y. V. Zubavichus, V. I. Zaikovskii, and S. A. Stepanov, *J. Magn. Magn. Mater.* **401**, 880 (2016).
- D. A. Balaev, S. S. Yakushkin, A. A. Dubrovskii, G. A. Bukhtiyarova, K. A. Shaikhutdinov, and O. N. Mart'yanov, *Tech. Phys. Lett.* **42**, 347 (2016).
- D. A. Balaev, A. A. Krasikov, A. A. Dubrovskii, A. D. Balaev, S. I. Popkov, V. L. Kirillov, and O. N. Mart'yanov, *J. Supercond. Nov. Magn.* **32**, 405 (2019).
- D. A. Balaev, A. A. Krasikov, D. A. Velikanov, S. I. Popkov, N. V. Dubynin, S. V. Stolyar, V. P. Ladygina, and R. N. Yaroslavtsev, *Phys. Solid State* **60**, 1973 (2018).
- S. Morup, D. E. Madsen, C. Fradsen, C. R. H. Bahl, and M. F. Hansen, *J. Phys.: Condens. Matter* **19**, 213202 (2007).
- Yu. L. Raikher and V. I. Stepanov, *J. Phys.: Condens. Matter* **20**, 204120 (2008).
- D. A. Balaev, A. A. Krasikov, A. A. Dubrovskiy, S. I. Popkov, S. V. Stolyar, O. A. Bayukov, R. S. Iskhakov, V. P. Ladygina, and R. N. Yaroslavtsev, *J. Magn. Magn. Mater.* **410**, 71 (2016).

39. S. I. Popkov, A. A. Krasikov, D. A. Velikanov, V. L. Kirillov, O. N. Martyanov, and D. A. Balaev, *J. Magn. Magn. Mater.* **483**, 21 (2019).
40. S. I. Popkov, A. A. Krasikov, A. A. Dubrovskiy, M. N. Volochaev, V. L. Kirillov, O. N. Martyanov, and D. A. Balaev, *J. Appl. Phys.* **126**, 103904 (2019).
41. R. H. Kodama and A. E. Berkowitz, *Phys. Rev. B* **59**, 6321 (1999).
42. N. J. O. Silva, A. Millan, F. Palacio, E. Kampert, U. Zeitler, and V. S. Amaral, *Phys. Rev. B* **79**, 104405 (2009).
43. D. A. Balaev, A. A. Krasikov, A. A. Dubrovskiy, S. I. Popkov, S. V. Stolyar, R. S. Iskhakov, V. P. Ladygina, and R. N. Yaroslavtsev, *J. Appl. Phys.* **120**, 183903 (2016).
44. E. C. Stoner and E. P. Wohlfarth, *Philos. Trans. R. Soc. London, Ser. A* **240**, 599 (1948).
45. P. Brázda, D. Nižánský, J.-L. Rehspringer, and J. P. Vejpravová, *J. Sol-Gel Sci. Technol.* **51**, 78 (2009).

Translated by E. Bondareva